BAND-LIMITED IMPULSE INVARIANCE METHOD USING LAGRANGE KERNELS

Nara Hahn

Institute of Sound and Vibration Research
University of Southampton, Southampton, UK
nara.hahn@soton.ac.uk

Frank Schultz and Sascha Spors

Institute of Communications Engineering
University of Rostock, Rostock, Germany
frank.schultz@uni-rostock.de
sascha.spors@uni-rostock.de

ABSTRACT

The band-limited impulse invariance method is a recently proposed approach for the discrete-time modeling of an LTI continuous-time system. Both the magnitude and phase responses are accurately modeled by means of discrete-time filters. It is an extension of the conventional impulse invariance method, which is based on the time-domain sampling of the continuous-time response. The resulting IIR filter typically exhibits spectral aliasing artifacts. In the band-limited impulse invariance method, an FIR filter is combined in parallel with the IIR filter, in such a way that the frequency response of the FIR part reduces the aliasing contributions. This method was shown to improve the frequency-domain accuracy while maintaining the compact temporal structure of the discrete-time model. In this paper, a new version of the band-limited impulse invariance method is introduced, where the FIR coefficients are derived in closed form by examining the discontinuities that occur in the continuous-time domain. An analytical anti-aliasing filtering is performed by replacing the discontinuities with band-limited transients. The band-limited discontinuities are designed by using the anti-derivatives of the Lagrange interpolation kernel. The proposed method is demonstrated by a wave scattering example, where the acoustical impulse responses on a rigid spherical scatter are simulated.

1. INTRODUCTION

Continuous-time systems are often modeled in the discrete-time domain by means of digital filters. A system function described in the Laplace domain (s-domain) is commonly discretized by converting it into the z-domain. Well-known textbook methods are the bilinear transform, the impulse invariance method, and the matched z-transform [1]. These methods typically suffer from spectral deviations due to frequency warping or spectral aliasing. Advanced methods for s-to-z mapping have been introduced to improve the frequency-domain accuracy of the discrete-time models [2–6]. In audio applications, some methods focus more on the magnitude response and allow phase distortions at high frequencies, which is acceptable considering spectral resolution of the human auditory system [7–10]. Other existing methods aim for an accurate modeling both in terms of magnitude and phase responses, which typically require higher filter orders [11, 12].

Another aspect of interest when assessing a discrete-time model is the transient properties (e.g. of the impulse responses and step responses). In a frequency-domain modeling, where the spectrum of a target system is sampled at discrete frequencies, the resulting impulse response usually exhibits smeared transient including pre- and post-ringing. If the continuous-time system has an infinite impulse response by nature (such as acoustic scattering, RLC circuits, and mass-spring systems), a frequency-domain modeling will exhibit temporal aliasing artifacts, as discussed in [13].

The band-limited impulse invariance method was introduced by the authors in [12]. A continuous-time system function described by partial fraction expansion is modeled by a parallel-structure filter consisting of infinite impulse response (IIR) and finite impulse response (FIR) filters. The IIR part is obtained by using the conventional impulse invariance method which is based on the time-domain sampling of the continuous-time impulse response [14]. The FIR filter is designed in such a way that it cancels the spectral aliasing caused by the IIR filters. In [12], an analytical approach is proposed for the FIR filter design. A closed-form expression is derived for a discrete-time sequence that achieves a perfect aliasing cancellation. Since the sequence is non-causal and infinitely long, it is approximated by applying a finite-length window function, yielding the FIR filter coefficients. A numerical version of the band-limited impulse invariance method is introduced in [15]. For this approach, the same IIR filter is used but the FIR filter is designed numerically by minimizing the spectral errors at control frequencies, constituting a least squares solution to an over-determined problem.

In this paper, we propose a new analytical version of the band-limited impulse invariance method. It is motivated by the fact that the spectral aliasing is caused by sampling a discontinuity in the time domain. A time-domain discontinuity typically exhibits an infinite frequency bandwidth. An anti-aliasing filtering is performed by replacing each discontinuity with a band-limited transient that is derived from a low-pass filter kernel. We employ the Lagrange interpolation filter whose continuous-time impulse response is described by a piece-wise polynomial. Since the FIR coefficients are described by polynomials, an efficient realization is possible. This is an advantage compared to the previous methods, where either the exponential integral functions have to be evaluated [12] or a matrix inversion has to be performed [15].

The fundamental idea of this band-limitation approach was initially introduced in the context of virtual analog modeling [16–18], where geometrically shaped waveforms (e.g. square waves and sawtooth waves) were synthesized by discrete-time systems. In the subsequent studies, this method was adopted for nonlinear system modeling [19]. A generalized treatment for higher-order discontinuities was introduced in [20], and was applied for the discrete-time realization of the radial functions in spherical harmonics expansions.

This paper is structured as follows. Sec. 2 introduces discontinuities of different orders and their analytical representations. The

band-limited impulse invariance method using the Lagrange kernel is presented in Sec. 3. The proposed method is evaluated by simulating the acoustical scattering of a rigid sphere. (Sec. 4). Sec. 5 concludes the paper.

2. HIGHER-ORDER DISCONTINUITIES

A time-domain sampling of a continuous-time signal with a given sampling frequency f_s (in Hz) introduces aliasing in the frequency domain, if the continuous-time signal has spectral components beyond the Nyquist limit ($|f| > \frac{f_\mathrm{s}}{2}$) [21]. The impulse response with an auto-regressive part typically exhibits a discontinuity at $t = 0$, which not only includes the jump discontinuity (here referred to as the 0th-order discontinuity) but also the discontinuities in the derivatives of different orders. The transient response $F_k(t)$ of a kth-order discontinuity can be represented by the $(k + 1)$th-order anti-derivative of the Dirac delta function [18],

$$F_0(t) = \int_{-\infty}^{t} \delta(\tau)\,\mathrm{d}\tau = u(t) \tag{1}$$

$$F_k(t) = \int_{-\infty}^{t} F_{k-1}(\tau)\,\mathrm{d}\tau = \frac{t^k}{k!}u(t), \tag{2}$$

where $u(t)$ denotes the Heaviside step function. The Laplace transforms of the respective discontinuity functions are given as [22]

$$\mathcal{L}\big\{F_k(t)\big\} = \frac{1}{s^{k+1}}, \tag{3}$$

corresponding to an integrator of order $k + 1$. The corresponding Fourier transform is obtained by evaluating (3) on the imaginary axis, whose magnitude decay at the rate of $-20{\cdot}(k{+}1)$ dB/decade. The spectral energy above the Nyquist limit thus decays faster for higher k.

We define the discontinuity of a given function $g(t)$ as the difference between the limit from the left and the limit from right to a point of interest,

$$\eta_0(t) = \lim_{\epsilon\to 0}\Big[g(t+\epsilon) - g(t-\epsilon)\Big]. \tag{4}$$

This can be extended to the derivatives of the function. Assuming that $g(t)$ is k-times differentiable, the kth-order discontinuity is defined as

$$\eta_k(t) = \lim_{\epsilon\to 0}\Big[g^{(k)}(t+\epsilon) - g^{(k)}(t-\epsilon)\Big], \tag{5}$$

where the shorthand notation

$$g^{(k)}(t) \coloneqq \tfrac{\mathrm{d}^k}{\mathrm{d}t^k} g(t) \tag{6}$$

is used for convenience. $\eta_0(t)$ in Eq. (4) corresponds to the 0th-order discontinuity as indicated by the subscript '0'.

The discontinuity analysis of a continuous-time impulse response is essential for the proposed band-limitation approach. In the following subsections, the higher-order discontinuities are derived for commonly used system functions. We consider causal and stable systems exclusively. Hence, the impulse response is right-sided and decays for $t \to \infty$. The real part of poles is always negative, and the region of conversion includes the imaginary axis [21]. Since the discontinuities at $t = 0$ are of our main interest, we will omit the time argument of the discontinuity (5) and use the notation $\eta_k(0) \to \eta_k$ in the remainder.

2.1. First-Order Section with a Single Pole

A first-order section system is described by a single pole $p \in \mathbb{C}$ and a residue $q \in \mathbb{C}$, whose Laplace-domain transfer function reads

$$G_\mathrm{FOS}(s) = \frac{q}{s-p} \tag{7}$$

and the corresponding impulse response is given as

$$g_\mathrm{FOS}(t) = q \cdot e^{pt} u(t). \tag{8}$$

The kth-order derivative of the impulse response reads

$$g^{(k)}_\mathrm{FOS}(t) = \begin{cases} q \cdot p^k \cdot e^{pt}, & t > 0 \\ 0, & t < 0. \end{cases} \tag{9}$$

which is continuous except for $t \neq 0$. Plugging (9) into (5) yields the discontinuity occurring at $t = 0$,

$$\eta_k = q \cdot p^k. \tag{10}$$

2.2. Second-Order Section with Complex Conjugate Poles

A second-order section is a sum of two first-order sections with complex conjugate poles and residues,

$$G_\mathrm{SOS}(s) = \frac{q}{s-p} + \frac{q^*}{s-p^*} \tag{11}$$

and the corresponding impulse response is

$$g_\mathrm{SOS}(t) = \left(q \cdot e^{pt} + q^* \cdot e^{p^* t}\right) u(t) \tag{12}$$

$$= 2|q|e^{\sigma_0 t}\cos(\omega_0 t + \phi_q)\, u(t), \tag{13}$$

where $q = |q| \cdot e^{i\phi_q}$ and $p = |p| \cdot e^{i\theta_p} = \sigma_0 + i\omega_0$. The imaginary unit is denoted by i. The kth-order derivative of the impulse response reads

$$g^{(k)}_\mathrm{SOS}(t) = \begin{cases} 2\,|q|\,|p|^k e^{\sigma_0 t}\cos\left(\omega t + \phi_q + k\theta_p\right), & t > 0 \\ 0, & t < 0. \end{cases} \tag{14}$$

The discontinuities at $t = 0$ are obtained by using (14) and (5), yielding

$$\eta_k = 2\,|q|\,|p|^k \cos(\phi + k\theta_p). \tag{15}$$

Eq. (15) can also be derived by using (10) for the complex conjugate poles and residues.

2.3. Multiple Poles

The partial fraction expansion of a system function may include multiple-pole terms [21, Ch. 4],

$$G_\mathrm{MUL}(s) = \frac{q}{(s-p)^{\mu+1}}, \tag{16}$$

where the pole multiplicity is $(\mu + 1)$. The corresponding impulse response is

$$g_\mathrm{MUL}(t) = q\,\frac{t^\mu}{\mu!} \cdot e^{pt} u(t). \tag{17}$$

The derivatives of the impulse response are

$$g_{\text{MUL}}^{(k)}(t) = \begin{cases} q\, e^{pt}\, t^{\mu-k} \sum_{l=0}^{k} \binom{k}{l} \frac{(pt)^l}{(\mu-k+l)!}, & t > 0 \\ 0, & t < 0, \end{cases} \tag{18}$$

with $\binom{k}{l} = \frac{k!}{l!(k-l)!}$ denoting the binomial coefficient. Following (5) and (18), the discontinuities at $t = 0$ are

$$\eta_k = \begin{cases} 0, & k < \mu \\ q \cdot \binom{k}{\mu} \cdot p^{k-\mu}, & k \geq \mu. \end{cases} \tag{19}$$

The impulse response of an $(\mu + 1)$th-order multi-pole system is thus continuous up to the $(\mu - 1)$th-order derivative.

3. BAND-LIMITATION USING LAGRANGE KERNEL

The underlying principle of the proposed method is to apply an anti-aliasing filter (low-pass filter) to the time-domain discontinuities. This is performed by replacing the discontinuity functions $F_k(t)$ with band-limited discontinuity functions $H_k(t)$. Analogous to (1) and (2), $H_k(t)$ is represented as an anti-derivative of a low-pass kernel $h_{\text{LPF}}(t)$,

$$H_0(t) = \int_{-\infty}^{t} h_{\text{LPF}}(\tau)\, \mathrm{d}\tau \tag{20}$$

which can be generalized to higher-order anti-derivatives,

$$H_k(t) = \int_{-\infty}^{t} H_{k-1}(\tau)\, \mathrm{d}\tau. \tag{21}$$

The difference between the full-band $F_k(t)$ and band-limited $H_k(t)$ discontinuities is called the residual function in the literature [17, 18],

$$D_k(t) \coloneqq H_k(t) - F_k(t). \tag{22}$$

The residual function $D_k(t)$ corresponds to the high-pass filtered component of the full-band discontinuity with reversed polarity (out-of-phase). Adding the residual function with the full-band discontinuity thus cancels the high-frequency components,

$$H_k(t) = F_k(t) + D_k(t), \tag{23}$$

yielding a band-limited impulse response that can be sampled with reduced aliasing. In the proposed method, the full-band discontinuity $F_k(t)$ and the residual function $D_k(t)$ are realized in the discrete-time domain by means of IIR filter and FIR filter, respectively. The output of the two filters exhibit the same aliasing artifacts but with opposite polarity. Therefore, superimposing the discrete-time sequences cancels the aliasing distortions. Following (1), (2), (21) and (22), it can be shown that the residual function is the anti-derivative of the difference between the low-pass kernel and the Dirac delta function,

$$D_0(t) = \int_{-\infty}^{t} \Big[h_{\text{LPF}}(\tau) - \delta(\tau) \Big]\, \mathrm{d}\tau \tag{24}$$

$$D_k(t) = \int_{-\infty}^{t} D_{k-1}(\tau)\, \mathrm{d}\tau. \tag{25}$$

It is of main interest to find a discrete-time model for the residual functions $D_k(t)$.

In this paper, we use the impulse response of a Lagrange interpolator as the low-pass filter kernel. Only odd-order Lagrange kernels are considered, as they are known to have superior spectral properties [23]. For a desired FIR length M, $M + 2$ equidistant nodes are placed between $-\frac{M+1}{2}T$ and $\frac{M+1}{2}T$, where the node distance is equal to the sampling period $T \coloneqq \frac{1}{f_s}$ The Lagrange kernel is defined within the $M + 1$ intervals as

$$h(t) = \frac{\prod_{\nu=0,\nu\neq\mu}^{M} (\frac{t}{T} + M - \mu - \nu)}{(-1)^{\mu}\, \mu!\, (M-\mu)!}, \tag{26}$$

if $\frac{t}{T} \in [-\frac{M+1}{2} + \mu, -\frac{M+1}{2} + \mu + 1]$ for $\mu = 0, \ldots, M$, and $h(t) = 0$, otherwise. It has a finite temporal support and is described by piece-wise polynomials. The band-limited discontinuities $H_k(t)$ are the anti-derivatives of the Lagrange kernel (26). The integration constants have to be chosen in such a way that $H_k(t)$ is continuous at the nodal points [18]. It is known that the frequency response of a Lagrange interpolation kernel exhibits maximum flatness at DC [23, 24]. Therefore, it can be integrated M times without causing instabilities. This allows us to use the Lagrange kernel for the band-limitation of higher-order discontinuities if $k \leq M$. Note that the resulting band-limited discontinuities $H_k(t)$ and the full-band discontinuities $F_k(t)$ (cf. (2)) have polynomial representations. The corresponding residual functions $D_k(t)$ are also described by piece-wise polynomials within the intervals. This allows an efficient realization of the residual functions.

The FIR coefficients are obtained by sampling the residual functions and scaling by the discontinuities η_k,

$$h^{(\text{FIR})}[n] = T \cdot \sum_{k=0}^{K} \eta_k \cdot D_k\big((n - \tfrac{M-1}{2}) \cdot T\big), \tag{27}$$

where n denotes the discrete-time sample index. The maximum discontinuity order (denoted by K) must be less than or equal to the Lagrange polynomial order M. Note that a group delay of $\frac{M-1}{2}$ samples is applied to ensure the causality of the filter. Finally, the overall filter is constructed by combining the FIR filter with the IIR filters,

$$G(z) = \sum_{m=0}^{M} h^{(\text{FIR})}[n] z^{-m} + z^{-\frac{M-1}{2}} \frac{qT}{1 - e^{pT} z^{-1}}. \tag{28}$$

The IIR part is obtained by applying the conventional impulse invariance method to a continuous system. A first-order system is considered for convenience. The IIR part is delayed by $\frac{M-1}{2}$ samples for a proper time alignment with the FIR part, which is crucial for the aliasing cancellation. The overall discrete-time model is thus delayed by $\frac{M-1}{2} \cdot T$ seconds compared to the continuous-time counterpart.

Note from (27) that the discontinuities η_k are the only terms that depend on the target system. The residual functions $D_k(t)$ can be pre-computed once the FIR length (or equivalently the Lagrange polynomial order) is chosen. The proposed method is thus suited for dynamic scenarios where the filter coefficients have to be changed constantly. This is a clear advantage in comparison with the previous methods. In the analytical approach [12] the exponential integral function has to be evaluated every time the target system is updated. The numerical approach [15] requires the computation of the pseudo inverse of a matrix.

4. EVALUATION

The performance of the proposed method is demonstrated by simulating the acoustical impulse responses of a point source evaluated at the surface of a rigid sphere. Such a configuration is often considered in spatial sound capture using spherical microphone arrays [25–27]. It is of importance to achieve a high spectral accuracy in terms of magnitude and phase, while preserving the temporal structure of the impulse responses.

The position of the point source is denoted by $\boldsymbol{x}_\mathrm{s} = (r_\mathrm{s}, \theta_\mathrm{s}, \phi_\mathrm{s})$ where r_s is the radius from the origin of the coordinate system, $\theta_\mathrm{s} \in [0, \pi]$ the colatitude angle from the z-axis, and $\phi_\mathrm{s} \in [0, 2\pi)$ the azimuth angle from the x-axis. The receiver position on the rigid sphere is denoted by $\boldsymbol{x} = (R, \theta, \phi)$ with R denoting the radius of the sphere. The acoustic transfer function from the source to the receiver can be expressed as a modal expansion ($r_\mathrm{s} > R$) [28, Sec. 4.2],

$$S(\boldsymbol{x}, \omega) = \sum_{\nu=0}^{\infty} \frac{2\nu+1}{4\pi} P_\nu(\cos\Theta_\mathrm{s}) \frac{-h_\nu(\frac{\omega}{c} r_\mathrm{s})}{\frac{\omega}{c} R^2 h_\nu'(\frac{\omega}{c} R)}, \tag{29}$$

where $P_\nu(\cdot)$ denotes the Legendre polynomial of order ν and $h_\nu(\cdot)$ the νth-order spherical Hankel function of the second kind. The prime symbol $(\cdot)'$ denotes the derivative with respect to the argument. The angle between $\boldsymbol{x}$ and $\boldsymbol{x}_\mathrm{s}$ is denoted by Θ_s. $\omega = 2\pi f$ denotes the angular frequency and c the speed of sound. The time harmonic term $e^{i\omega t}$ is omitted for brevity. By exploiting the explicit formula [29, Eq. (10.49.7)] and the recurrence relation [29, Eq. (10.51.2)] of the the spherical Hankel functions, (29) can be expressed in the Laplace domain as [13]

$$S(\boldsymbol{x}, s) = \frac{c}{4\pi r_\mathrm{s} R} e^{-\frac{r_\mathrm{s}-R}{c} s} \sum_{\nu=0}^{\infty} (2\nu+1) P_\nu(\cos\Theta_\mathrm{s}) A_\nu(s) \tag{30}$$

which is the analytic continuation in the complex plane (i.e. $i\omega$ is substituted with s). The modal spectrum $A_\nu(s)$ can be described by a fractional function or a partial fraction expansion,

$$A_\nu(s) = \frac{\sum_{k=0}^{\nu} \beta_{\nu,k} (\frac{r_\mathrm{s}}{c})^{k-n} s^k}{\sum_{k=0}^{\nu+1} \gamma_{\nu,k} (\frac{R}{c})^{k-n-1} s^k} \tag{31}$$

$$= \sum_{k=0}^{\nu} \frac{q_{\nu,k}}{s - p_{\nu,k}}. \tag{32}$$

Please refer to [13, 15] for a thorough derivation. The poles and zeros of the system function respectively correspond to the roots of the denominator and numerator of $A_\nu(s)$. As depicted in Fig. 1, the poles and zeros are distinct and their real parts are negative. The partial fraction expansion (32) constitutes a parallel-structure filter which consists of first- and second-order section filters. The system function (31) can also be realized as a cascaded system as discussed in [30].

The continuous-time system (32) is now modeled by the proposed band-limited impulse invariance method. The radius of the rigid sphere is assumed to be $R = 0.042\,\mathrm{m}$. The Lagrange polynomial order is set to $M = 15$, which corresponds to an FIR length of $L_\mathrm{FIR} = 15$ taps. A band limitation is applied up to the 10th-order discontinuity ($K = 10$). The simulation is performed at the sampling rate of $48\,\mathrm{kHz}$. The speed of sound is assumed to be $c = 343\,\mathrm{m/s}$.

The following methods are considered for comparison. The respective abbreviations will be used in the remainder.

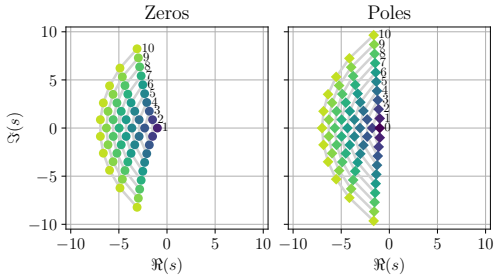

Figure 1: Laplace-domain zeros and poles describing the modal transfer functions on a rigid sphere, cf. (29)–(32). The zeros correspond to the roots of the spherical Hankel functions $h_n(\cdot)$ and the poles to the roots of their derivatives $h_n'(\cdot)$. Zeros/poles for the same orders ($\nu = 0, \ldots, 10$) are connected with gray lines. For the ease of visualization, $\frac{r_\mathrm{s}}{c} = \frac{R}{c} = 1$ is considered. Note that only the poles are directly used by the proposed discrete-time model. The effect of the zeros are implicitly included via the residues $q_{\nu,k}$ of the partial fraction expansion (32).

- The conventional impulse invariance method (IIM), which is based on time-domain sampling [14]. The discrete-time model has only IIR filters.
- The analytical band-limited impulse invariance method (A-BLIIM) [12]. The FIR coefficients are given in a closed form described by the exponential integral functions.
- The numerical version of the band-limited impulse invariance method (N-BLIIM) [15]. The FIR coefficients are computed in a least-square-error sense. The spectral errors are minimized at $2 \times L_\mathrm{FIR}$ control frequencies that are logarithmically distributed between 2 Hz and 24 kHz.
- The proposed band-limited impulse invariance method using Lagrange polynomial kernel (P-BLIIM).
- Frequency-sampling method (FSM), where the desired modal spectrum (29) is sampled at 2^{16} uniform frequencies [31]. The modal impulse response is then obtained by the inverse discrete Fourier transform.

All methods except for FSM have the same IIR filters that are designed by IIM. For a fair comparison, the same FIR length is used for the three band-limited impulse invariance methods (A-BLIIM, N-BLIIM, and P-BLIIM).

Fig. 2 shows the modal spectra ($\nu = 0, \ldots, 10$) resulting from the discrete-time models. The magnitude spectra are depicted in the top row and the corresponding spectral errors in the bottom row. The original spectra (29) are shown as a reference in Fig. 2(a). The FSM exhibits a perfect spectral accuracy by design, thus the magnitude responses are identical to those in Fig. 2(a). For the N-BLIIM (Fig. 2(d)), the control frequencies are indicated by black crosses '×' in the bottom row. It can be seen that the discrete-time model by the IIM have excessive magnitude responses near the Nyquist limit, which is due to aliasing artifacts. The spectral distortion increases for higher modal orders. This is attributed to the fact that the imaginary part of the poles is getting closer to the Nyquist frequency thereby causing more aliasing artifacts, cf. Fig. 1(right). It is worth noting that, for the IIM, the spectral deviation is spread throughout the whole frequency band. Since the continuous-time spectrum decays rather slowly

($-20\,\mathrm{dB/decade}$), the spectral repetitions due to aliasing have a global effect. The results for the band-limited impulse invariance methods (A-BLIIM, N-BLIIM, and P-BLIIM) clearly show the benefit of using an FIR filter in addition to the IIR filter, cf. Fig. 2(c), Fig. 2(d), and Fig. 2(e). The magnitude responses near the Nyquist frequency are in a close agreement with the desired spectra. In comparison with the result of the IIM, the spectral deviations are reduced considerably. In terms of spectral accuracy, both N-BLIIM and P-BLIIM outperform the A-BLIIM below $10\,\mathrm{kHz}$. The performances at higher frequencies are similar to each other. While the spectral deviations for P-BLIIM change more gradually over frequency, the accuracy of N-BLIIM is strongly dependent on the distribution of the control frequencies which is often chosen heuristically. The increased spectral deviations near the Nyquist limit can be explained by the fact that the anti-aliasing filter is not ideal and has a gradual transition between the pass-band and stop-band. As depicted in Fig. 3, the spectral accuracy of P-BLIIM can be improved by increasing the FIR filter length. Discrete-time models with longer FIR filters achieves better accuracy near the Nyquist limit. The improvement comes at the expense of a longer non-causal part in the impulse responses.

In order to investigate the temporal properties of different models, the impulse responses on the sphere are examined. The impulse response of each mode is first computed by exciting the discrete-time filters with a discrete-time impulse $\delta[n]$. For the FSM, the modal impulse responses are obtained by computing the inverse discrete Fourier transform of the modal spectra. The individual modal impulse responses are then linearly combined using the modal expansion, analogous to (29) and (30). The expansion is computed up to the 10th order. A point source is placed on the x-axis with $1\,\mathrm{m}$ distance from the origin ($r_\mathrm{s} = 1\,\mathrm{m}, \theta_\mathrm{s} = 90^\circ, \phi_\mathrm{s} = 0^\circ$), and receivers are arranged along the equator of the sphere ($R = 0.042\,\mathrm{m}, \theta = 90^\circ, \phi \in [-180^\circ, 180^\circ]$). Note from (30) that the wave propagation from the source to the nearest point on the sphere corresponds to a delay of $\frac{r_\mathrm{s}-R}{c}$. Since the delay is generally not an integer multiple of the sampling period T, a fractional delay filter might be needed for an accurate discrete-time modeling [32]. However, this is beyond the scope of this paper, and we assume that the delay is ideally modeled. Our focus is on the evaluation of the modal responses, represented by $A_\nu(s)$ in (30).

Figure 4 shows the directional impulse responses at the receiver positions. The absolute amplitudes are depicted in dB-scale as indicated by the color-map. The considered discrete-time models exhibit different delays. For visualization purposes, the impulse responses are aligned and the time axes are adjusted accordingly. The time-of-arrival of the first impulse on the sphere is $t_\mathrm{TOA} = \frac{r_\mathrm{s}-R}{c} \approx 2.973\,\mathrm{ms}$, which coincides with the onset of the impulse responses for IIM. For the band-limited approaches (A-BLIIM, N-BLIIM, and P-BLIIM), there are components that arrive earlier than the theoretical time-of-arrival t_TOA. These non-causal parts correspond to the left-half of the FIR filters, which precede the IIR filter by $\frac{L_\mathrm{FIR}-1}{2} = 7$ samples or $\tau_\mathrm{FIR} = \frac{L_\mathrm{FIR}-1}{2} \cdot T \approx 0.146\,\mathrm{ms}$. The influence of the FIR filters are observed within the interval $t \in [t_\mathrm{TOA} - \tau_\mathrm{FIR}, t_\mathrm{TOA} + \tau_\mathrm{FIR}]$, where minor differences can be seen among the three methods. Since the same IIR filters are used by all methods except for FSM, the impulse responses are identical for $t > t_\mathrm{TOA} + \tau_\mathrm{FIR}$. The FSM yields considerably different results. The impulse responses exhibit strong pre- and post-ringing spanned over the entire time range. In the later part of the impulse response ($t > 3.5\,\mathrm{ms}$), the post-ringing dominates the actual impulse response because it decays slower than the latter. The spatio-temporal structure of the impulse response is hardly identifiable.

The results show that FSM and IIM are two extreme cases. The FSM achieves a perfect spectral accuracy at the expense of strong temporal artifacts. The IIM models the temporal profile of the impulse response accurately but the resulting frequency response deviates from the original spectrum. In both methods, increasing the sampling frequency mitigates the problems. The resulting discrete-time models then become similar to each other [30]. The band-limited impulse invariance methods can be used to balance between the temporal and spectral fidelity. The discrete-time model can be configured straightforwardly by varying the Lagrange polynomial order and the maximum discontinuity order that needs to be low-pass filtered. Increasing the length of the FIR improves the accuracy in the frequency domain. A shorter FIR filter might be preferred if a compact transient response is of interest.

5. CONCLUSION

A new version of the band-limited impulse invariance method is presented. The proposed discrete-time model relies on the partial fractional expansion of the system function in the Laplace domain. The resulting discrete-time model is a parallel combination of FIR and IIR filters. The IIR filter is obtained by using the conventional impulse invariance method which typically produces aliasing artifacts. The FIR filter is then used to cancel the spectral distortion caused by the aliasing. The FIR coefficients are derived based on the discontinuity analysis of the continuous-time impulse response. By using the Lagrange kernel which is described by piece-wise polynomials, an analytical low-pass filtering is applied to time-domain discontinuities of different orders. Since the FIR filter coefficients are described by polynomials, the implementation requires low computational complexity. Moreover, the filter can be constructed by linearly combining pre-computed sequences which correspond to the so-called residual functions. If the target system changes, only the discontinuity coefficients have to be updated. This facilitates an efficient realization in dynamic scenarios. The performance of the method is demonstrated by simulating the acoustical scattering of a rigid sphere. It was shown to be comparable with the analytical and numerical versions of the band-limited impulse invariance methods that have been previously introduced.

6. REFERENCES

[1] J. G. Proakis and D. G. Manolakis, *Digital Signal Processing: Principles, Algorithms, and Applications*. Prentice-Hall, 1996.

[2] M. A. Al-Alaoui, "Novel stable higher order s-to-z transforms," *IEEE Trans. Circuits Syst. I*, vol. 48, no. 11, pp. 1326–1329, 2001.

[3] ——, "Novel approach to analog-to-digital transforms," *IEEE Trans. Circuits Syst. I*, vol. 54, no. 2, pp. 338–350, 2007.

[4] J. Flynn and J. D. Reiss, "Improving the frequency response magnitude and phase of analogue-matched digital filters," in *Proc. 144th Audio Eng. Soc. (AES) Conv.*, Milan, Italy, May 2018.

[5] D. W. Gunness and O. S. Chauhan, "Optimizing the magnitude response of matched z-transform filters ("MZTI") for

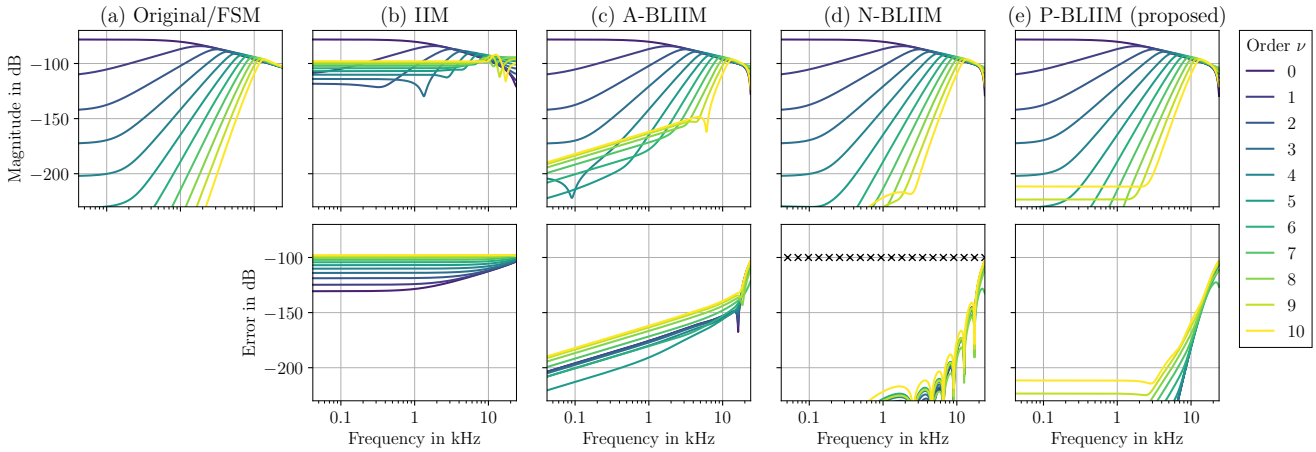

Figure 2: The frequency responses of the individual modes on a rigid sphere (rigid sphere radius $R = 0.042\,\mathrm{m}$, point source radius $r_\mathrm{s} = 1\,\mathrm{m}$, modal orders $\nu = 0, \ldots, 10$, FIR length $L_\mathrm{FIR} = 15$, sampling frequency $f_\mathrm{s} = 48\,\mathrm{kHz}$). The desired spectra are shown on the top left (a), which is identical to the results for FSM. Columns (b)–(e) depict the results for different discrete-time models (IIM, A-BLIIM, N-BLIIM, and P-BLIIM). The top row shows the magnitude spectra of the individual modes, and the bottom row shows the corresponding spectral deviations. The crosses '×' in (d) indicate the control frequencies used by N-BLIIM ($2 \times L_\mathrm{FIR}$ frequencies; logarithmic distribution from 2 Hz to 24 kHz).

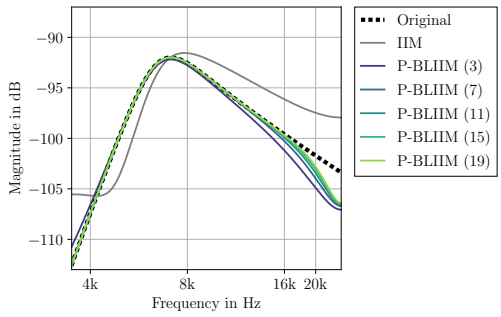

Figure 3: Modal spectrum of order $\nu = 5$. Discrete-time models designed by P-BLIIM are compared with the original spectrum and the model by IIM. Different FIR filter lengths ($L_\mathrm{FIR} = 3, 7, 11, 15$, and 19) are considered for P-BLIIM, as indicated by the numbers in in the legend. In order to highlight the performance near the Nyquist limit ($\frac{f_\mathrm{s}}{2} = 24\,\mathrm{kHz}$), only the high-frequency spectra are shown.

loudspeaker equalization," in *Proc. 32nd Audio Eng. Soc. (AES) Int. Conf.*, Hillerød, Denmark, Sep. 2007.

[6] C. C. Darabundit, J. S. Abel, and D. Berners, "Nyquist band transform: An order-preserving transform for bandlimited discretization," *J. Audio Eng. Soc. (JAES)*, vol. 70, no. 9, pp. 674–689, 2022.

[7] S. J. Orfanidis, "Digital parametric equalizer design with prescribed Nyquist-frequency gain," *J. Audio Eng. Soc. (JAES)*, vol. 45, no. 6, pp. 444–455, 1997.

[8] M. Massberg, "Digital low-pass filter design with analog-matched magnitude response," in *Proc. 131st Audio Eng. Soc. (ASE) Conv.*, New York, NY, USA, Oct. 2011.

[9] T. Schmidt and J. Bitzer, "Digital equalization filter: New solution to the frequency response near Nyquist and evaluation by listening tests," in *Proc. 128th Audio Eng. Soc. (AES) Conv.*, London, UK, May 2010.

[10] D. P. Berners and J. S. Abel, "Discrete-time shelf filter design for analog modeling," in *Proc. 115th Audio Eng. Soc. (AES) Conv.*, New York, NY, USA, Oct. 2003.

[11] S. Särkkä and A. Huovilainen, "Accurate discretization of analog audio filters with application to parametric equalizer design," *IEEE Trans. Audio Speech Lang. Process.*, vol. 19, no. 8, pp. 2486–2493, 2011.

[12] N. Hahn, F. Schultz, and S. Spors, "Band limited impulse invariance method," in *Proc. 30th Eur. Signal Process. Conf. (EUSIPCO)*, Belgrade, Serbia, Sep. 2022, pp. 209–213.

[13] ——, "Aliasing-free time-domain simulation of spherical microphone arrays," in *Proc. 49th German Annu. Conf. Acoust. (DAGA)*, Hamburg, Germany, Mar. 2023, pp. 1620–1623.

[14] R. A. Gabel and R. A. Roberts, *Signals and Linear Systems*, 3rd ed. Wiley, 1986.

[15] N. Hahn, F. Schultz, and S. Spors, "Accurate time-domain simulation of spherical microphone arrays," in *Proc. 10th Forum Acusticum*, Torino, Italy, Sep. 2023, pp. 599–606.

[16] T. Stilson and J. O. Smith, "Alias-free digital synthesis of classic analog waveforms." in *Proc. Int. Comput. Music Conf.*, Hong Kong, Aug. 1996.

[17] V. Välimäki and A. Huovilainen, "Antialiasing oscillators in subtractive synthesis," *IEEE Sig. Process. Mag.*, vol. 24, no. 2, pp. 116–125, 2007.

[18] V. Välimäki, J. Pekonen, and J. Nam, "Perceptually informed synthesis of bandlimited classical waveforms using integrated polynomial interpolation," *J. Acoust. Soc. Am. (JASA)*, vol. 131, no. 1, pp. 974–986, 2012.

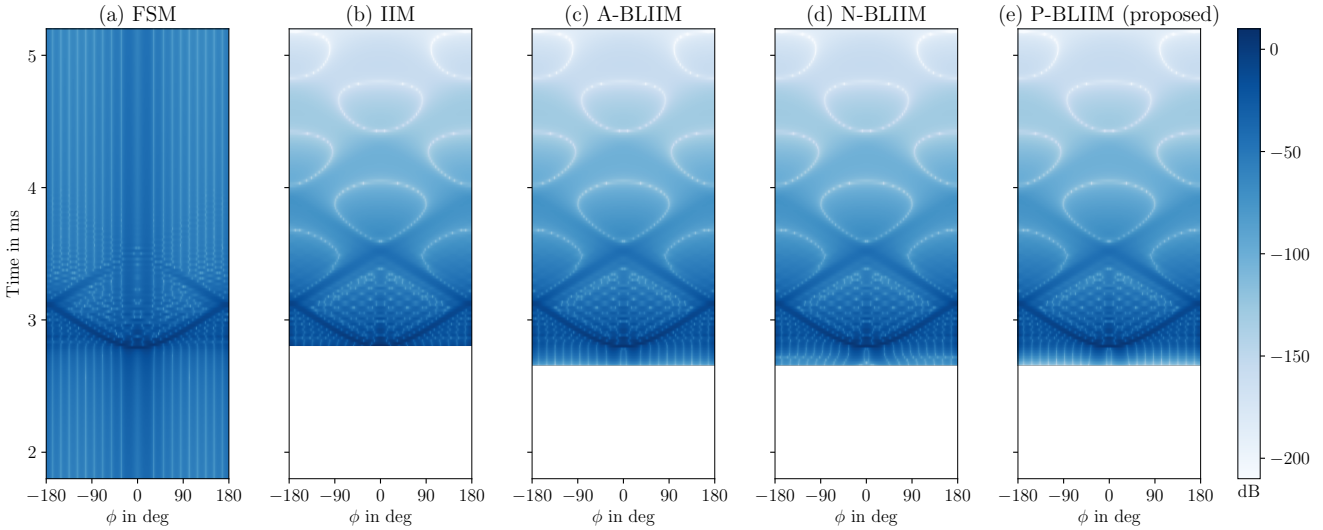

Figure 4: Directional impulse responses of a point source ($r_\mathrm{s} = 1\,\mathrm{m}$, $\theta_\mathrm{s} = 90°$, $\phi_\mathrm{s} = 0°$) on a rigid sphere ($R = 0.042\,\mathrm{m}$, $\theta = 90°$, $\phi \in [-180°, 180°]$). The band-limited approaches (A-BLIIM, N-BLIIM, and P-BLIIM) are implemented with the same FIR length $L_\mathrm{FIR} = 15$. The considered discrete-time models have different non-causal lengths. The time axes are adjusted so that the impulse responses from different methods are aligned. The time-of-arrival of the first impulse on the surface ($\theta = 0°$, $\phi = 0°$) is $t_\mathrm{TOA} = \frac{r_\mathrm{s} - R}{c} \approx 2.973\,\mathrm{ms}$.

[19] F. Esqueda, V. Välimäki, and S. Bilbao, "Rounding corners with BLAMP," in *Proc. Int. Conf. Digit. Audio Effects (DAFx)*, Brno, Czech Republic, Sep. 2016, pp. 121–128.

[20] N. Hahn, F. Schultz, and S. Spors, "Higher order antiderivatives of band limited step functions for the design of radial filters in spherical harmonics expansions," in *Proc. 24th Int. Conf. Digital Audio Effects (DAFx)*, Online, Sep. 2021, pp. 184–190.

[21] B. Girod, R. Rabenstein, and A. Stenger, *Signals and Systems*. Wiley, 2001.

[22] A. V. Oppenheim, R. W. Schafer, and J. R. Buck, *Discrete-Time Signal Processing*. Prentice Hall, 1999.

[23] A. Franck and K. Brandenburg, "A closed-form description for the continuous frequency response of Lagrange interpolators," *IEEE Sig. Process. Lett.*, vol. 16, no. 7, pp. 612–615, 2009.

[24] V. Välimäki, "Discrete-time modeling of acoustic tubes using fractional delay filters," Ph.D. dissertation, Helsinki University of Technology, Espoo, Finland, 1995.

[25] B. Rafaely, *Fundamentals of Spherical Array Processing*. Springer, 2015.

[26] B. Bernschütz, C. Pörschmann, S. Spors, and S. Weinzierl, "SOFiA sound field analysis toolbox," in *Proc. Int. Conf. Spatial Audio (ICSA)*, Detmold, Germany, Nov. 2011, pp. 7–15.

[27] D. P. Jarrett, E. A. P. Habets, M. R. P. Thomas, and P. A. Naylor, "Rigid sphere room impulse response simulation: Algorithm and applications," *J. Acoust. Soc. Am. (JASA)*, vol. 132, no. 3, pp. 1462–1472, 2012.

[28] N. A. Gumerov and R. Duraiswami, *Fast Multipole Methods for the Helmholtz Equation in Three Dimensions*. Elsevier, 2005.

[29] F. W. J. Olver, D. W. Lozier, R. F. Boisvert, and C. W. Clark, *NIST Handbook of Mathematical Functions Handback*. Cambridge University Press, 2010.

[30] N. Hahn, F. Schultz, and S. Spors, "Spatio-temporal properties of simulated impulse responses on a rigid sphere," in *Proc. 47th German Annu. Conf. Acoust. (DAGA)*, Vienna, Austria, Aug. 2021.

[31] L. R. Rabiner and B. Gold, *Theory and Application of Digital Signal Processing*. Englewood Cliffs: Prentice Hall, 1975.

[32] T. I. Laakso, V. Valimaki, M. Karjalainen, and U. K. Laine, "Splitting the unit delay," *IEEE Sig. Process. Mag.*, vol. 13, no. 1, pp. 30–60, 1996.